



## Device characterization and cross-layer protocol design for RF energy harvesting sensors

Prusayon Nintanavongsa<sup>a,\*</sup>, Rahman Doost-Mohammady<sup>a</sup>, Marco Di Felice<sup>b</sup>,  
Kaushik Chowdhury<sup>a</sup>

<sup>a</sup> Department of Electrical and Computer Engineering, Northeastern University, Boston, MA 02115, United States

<sup>b</sup> School of Computer Science, University of Bologna, Bologna, Italy

### ARTICLE INFO

#### Article history:

Available online 9 October 2012

#### Keywords:

Energy harvesting  
Sensor networks  
Duty cycle  
Routing  
Ambient radio frequency

### ABSTRACT

Energy harvesting from ambient radio frequency waves has the potential for realizing long lived wireless sensor networks, by reducing their dependence on the limited and irreplaceable on-board batteries. We propose two cross-layer approaches, called device-agnostic (DA) and device-specific (DS) protocols, for such networks composed of energy harvesting boards connected to off-the-shelf available sensors. These protocols determine the routing paths and the harvesting-transmission duty cycle at each hop under different conditions. The DA scheme relies purely on the local measurements on the harvesting capability of a node after the sensors are deployed, and is useful for single-flow networks. The DS scheme provides a joint hardware–software optimization by allowing the selection of the energy storing capacitor, apart from the route and duty cycle determination. Both schemes rely on a rich set of device-level experimental studies that help provide exact performance characteristics in practical scenarios, and results reveal significant performance improvement over other existing schemes.

© 2012 Elsevier B.V. All rights reserved.

### 1. Introduction

Wireless sensor networks (WSNs) are widely considered the technology of choice for different types of monitoring, data gathering, surveillance, and appliance control applications, among others [1]. However, one of the most important factors preventing the extensive use of WSNs is that the lifetime of the network, i.e., the duration of the services it provides, is severely limited by energy resources. The sensor nodes are powered by short-lived batteries whose replacement or recharge is expensive and environmentally unfriendly, if even possible. Therefore, human assistance for battery replacements is needed, and this severely limits the monitoring applications that can be effectively performed by WSNs [2]. Moreover, as these networks get pervasive and tightly integrated into daily lives, the power drawn by thousands of nodes for their continuous operation cannot be ignored. In fact, efficient utilization of available energy resources is one of the fundamental challenges of the current century. The world energy consumption is expected to increase by 49% total, or 1.4% per year, from 495 quadrillion British thermal units (Btu) in year 2007 to 739 quadrillion Btu in year 2035 [3], and the steadily growing telecommunication sector is a major consumer of the energy resource. Thus, there is a strong motivation to integrate current WSN technology with an energy harvesting capability that would allow a sensor to replenish part or all of its operational costs, and render it “perennial” from an energy point of view [4].

\* Corresponding author.

E-mail addresses: [prusayon@ece.neu.edu](mailto:prusayon@ece.neu.edu) (P. Nintanavongsa), [doost@ece.neu.edu](mailto:doost@ece.neu.edu) (R. Doost-Mohammady), [difelice@cs.unibo.it](mailto:difelice@cs.unibo.it) (M. Di Felice), [krc@ece.neu.edu](mailto:krc@ece.neu.edu) (K. Chowdhury).

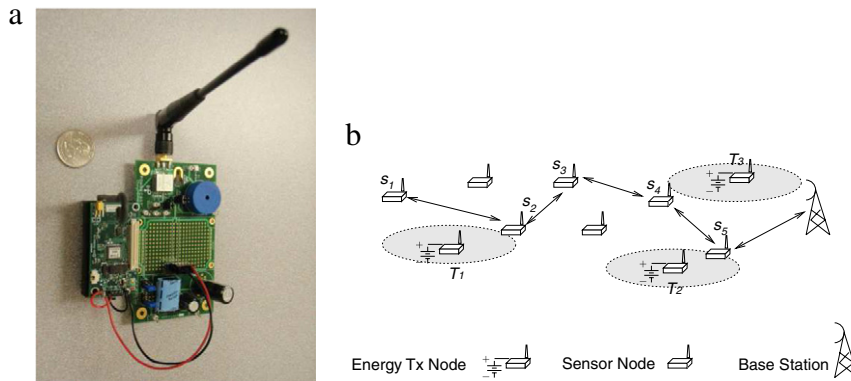


**Fig. 1.** The RF powered sensor (a) and the network architecture (b).

In many envisaged applications of WSNs, the nodes are deployed indoors, or embedded in living spaces. In most indoor deployments, the nodes may be unable to access some of the non-conventional sources of energy extensively investigated in previous research, such as solar [5], wind [6] and vibration [7]. Instead, we assume a WSN that can harvest energy from ambient radio frequency (RF) waves, which can be generated by existing wireless networks used in homes and offices, or by specialized high power wireless transmitters that intermittently emit RF radiation. Recently prototypes for such RF harvesters have been developed in academia [8–10], as well as commercial products have been introduced by the industry [11]. A complete energy harvesting sensor formed by interfacing the harvesting module from [11] with a Mica2 mote is shown in Fig. 1(a).

While advances have been made in device design for RF powered sensors, network protocols that support these devices are still in a nascent stage. Each node receives a different amount of RF energy based on its distance from the wireless transmitter, and this too is dependent on the wireless channel conditions and the conversion efficiency of the specific circuit. For these nodes, energy savings are not obtained just by alternating between predictable “awake” and “asleep” states [12], but also through considering the (expected) energy that a node might have at a later time. Additionally, the route management must consider both the long-term suitability of a node to harvest energy by virtue of its location, and its current residual level of energy. How to tradeoff the charging characteristics of a particular device, and the requirement of keeping the entire end to end path connected with sufficient energy at each node is another key challenge.

In this paper, we propose two cross-layer protocols that assign a charging–discharging cycle to each node at the link layer, and then identify the best possible route from the source node to the sink. We call these as (i) *device-agnostic* (DA), and (ii) *device-specific* (DS) protocols, each of which is suited to a different application scenario. The network architecture is described in Fig. 1(b), with the sensors deployed randomly in the study area. The RF sources are represented by  $T_1$ ,  $T_2$ , and  $T_3$  that are connected to a power source. Each of these power transmitters is effective within a coverage region, shown in the figure by shaded circular regions. Both the DA and DS protocols aim to find the path from node  $s_1$  to base station under the following different conditions.

### 1.1. Device-agnostic protocol

This method allows each node to independently identify its energy harvesting capability, in terms of the time to charge its storage capacitor. The routing metric uses this time, which we have experimentally determined to be a function of the node location, to decide the suitability of the node's participation in a route. The advantage of this method is that it not only eliminates the need for fine grained study of the specific received RF power at the node antenna, but also it is independent of the type and characteristics of the harvesting module used with the mote (hence, *device-agnostic*). All the nodes of the path follow the optimal charging–transmission cycle (even if their own charging times may disagree). In DA, the optimal route and duty cycle are tailored for the source to destination nodes. Consequently, the DA protocol yields the optimal result if all routes in the WSN are completely non-overlapping. However, it is possible that nodes in the route also belong to other routes. In this case, the optimality of DA is not guaranteed since nodes that participate in more than one route may encounter premature energy depletion. A preliminary study of this method is presented in [13].

### 1.2. Device-specific protocol

This method allows any routes to be formed, without restrictions. It creates a single network-wide schedule that allows each node to transmit and re-charge with exact synchronization. However, it requires a meticulous characterization of the harvesting circuit, knowledge of the received power value, operational power usages for the sensor, the rate of energy storage capacitor discharge during charging, transmission, and reception, among other parameters, which can either be obtained through measurements or through manufacturer's specifications (hence, *device-specific*). We describe a carefully

performed study of the Mica2 mote interfaced with the Powerharvester receiver to formulate a joint PDF of energy availability for a given node. Finally, such characterization curves for all the sensors are then combined at the base station to identify the best schedule for the network. A key benefit of the DS scheme over the DA scheme comes from the joint optimization of the hardware of the energy harvesting sensor (i.e., the choice of the capacitor) and the other network parameters, such as the duty cycle. Hence, application requirements, such as bounds on path latency, can be mapped much better to the WSN deployment, as this method provides an additional control on the design, instead of the pure network-only decisions.

The rest of the paper is organized as follows. Related work on protocol design for energy harvesting sensors is given in Section 2. The first approach, i.e., the device-agnostic approach is described in Section 3. The proposed device-specific protocol is given in Section 4. The performance evaluation is undertaken in Section 5, and concluding remarks are presented in Section 6.

## 2. Related work

Maximizing the steady state data flow from the source node to the destination, under constraints of power, bandwidth, and the rate of harvesting is explored in [14]. The proposed self-adapting maximum flow (SAMF) routing strategy finds feasible paths while automatically adapting to time-varying operating conditions. The routing algorithm always route packets across the path with maximum residual capacity to the sink. The complexity of the routing algorithm is hidden behind the real-time computation of residual path capacities. In principle, in fact, routing metrics should be recomputed at each node (and possibly diffused) whenever a data packet is processed or an environmental change is detected. This poses a huge computational power to the sensors which are in essence very short in harvested power. A geographic routing protocol D-APPOLO for asynchronous energy-harvesting WSNs is proposed in [15]. It periodically and locally calculates the duty cycle of each node, based on an estimated energy budget for each period which includes the currently available energy, the predicted energy consumption, and the energy expected from the harvesting device assuming solar cells rated at 200–300 mW h. For the algorithm to work, the sender must know the duty cycle of the receiver in advance, and can then wait for the receiver to be ready to receive the packet. The energy aware distance vector routing (EADV) protocol is devised for sensor motes that are powered by small solar cells and use capacitors for storage [16]. One of the factors influencing the route decision is a cost metric, which is determined by the overhead of gathering the energy. For the capacitor, the quality factor ( $Q$ -value) determines the energy loss rate within the device, and therefore routes must be chosen that minimize  $Q$  to prevent waste of energy. However, this scheme does not address the performance metrics of the network, e.g. the throughput, delay, among others. Pappa et al. [17] incorporates the node's residual voltage  $V_{res}^i$  into the route forming decision in AODV (in addition to the classical sequence number and hop count) so that the final selected route has the longest lifetime. Each node  $i$  maintains its own fractional residual voltage value, which serves as the decision metric, as  $\frac{V_{full}}{V_{res}^i}$ . During route formation a summation of the above metric for the nodes in the path is calculated, and the path with lowest cost, i.e.,  $\sum_{vi} \frac{V_{full}}{V_{res}^i}$ , is chosen. Thus, nodes that have a lower cost metric, i.e., lower residue voltage ratio, will be more favorable during route formation in the VA scheme.

At the link layer, there have been several efforts towards identifying optimal charging–transmission cycles. Kansal et al. [18] analyzed the requirements for “energy neutral”, i.e., matching energy consumption to production. Also an attempt has been made to model the energy source and to adjust the energy of the node's duty cycle based on the expected available energy. At the beginning of each slot, the node evaluates its received power from the energy source and also the power drawn by the load. If the actual received power is less than the predicted received power, the duty cycle will be reduced gradually in the next cycles to compensate for the shortage of energy. In the opposite case, we want to increase the duty cycles used in the future to utilize the excess energy received in the recent time slot. This method only discusses finding the optimal duty cycle and it does not provide the details of how to use the duty cycle in a networked fashion. In addition to dynamic duty cycling algorithms, [12] analyzed the performance of the conventional MAC schemes like CSMA and ID Polling on WSNs with ambient energy harvesting capabilities. This work shows the ineffectiveness of conventional MAC schemes for ambient energy harvesting capabilities and the need for the design of new schemes.

## 3. Device-agnostic (DA) protocol

We describe the proposed DA scheme by first mapping the charging time of the energy harvesting circuit to the distance of the energy transmitter (ET). Then, we present the route formation scheme that uses the charging capability of a sensor as the metric. Finally, the duty cycle at the link layer is chosen for the nodes in the path through a linear optimization.

### 3.1. Relationship of charging time and distance

In this section, we determine experimentally the charging time for a given commercially available wireless energy transfer device, by the following steps:

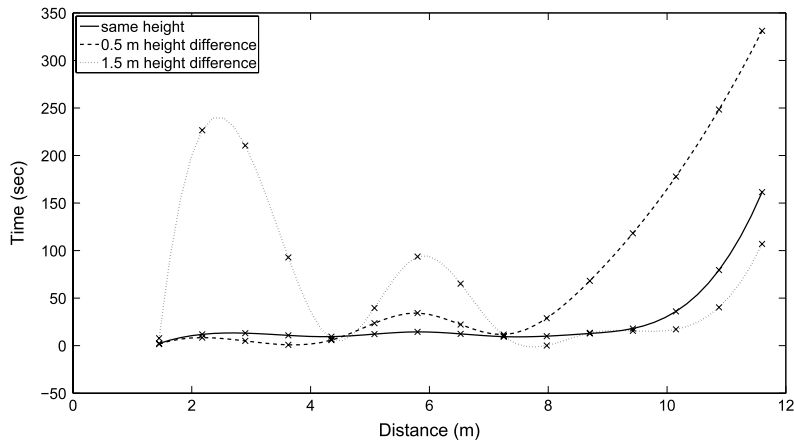


**Fig. 2.** Variation of the charging time of a capacitor on the receiver as a function of increasing distance for different transmitter–receiver heights.

### 3.1.1. Experimental setup

Our experimental apparatus consists of a P2100 energy harvesting module from Powercast Co. [11], which operates in the 900 MHz ISM band, and is composed of an energy transmitter (ET) and receiver boards. The receiver converts the energy of the transmitted continuous wave 3 W signal sent by the ET to DC voltage with the help of a 1 mF capacitor. This stored energy in the capacitor can then be used to re-charge standard batteries as the load, or directly for sensor operation. We compared the charging rates of the capacitor from 0 to 1.16 V, with the latter being a hardware enforced upper limit, for different transmitter–receiver separation distances in the range [1.5, 12] m. The experiments were conducted in a long corridor of our research building that simulated a tunnel-like behavior. Moreover, at each chosen distance, three different relative heights between the ET and the receiver were chosen as follows: (i) same height, (ii) receiver 0.5 m higher than ET, and (iii) receiver 1.5 m higher than ET, respectively.

### 3.1.2. Observations

The results of our experiments are shown in Fig. 2 with the time for charging on the Y-axis, and the separation distance on the X-axis. Firstly, as a limiting condition, we observed that at distances greater than 12 m, the charging takes an infinite length of time, since the capacitor does not get to the maximum charge voltage at all. Thus, we assume this distance as the upper limit for the current type of energy transferring devices. Irrespective of the relative heights between the ET and the receiver, the general trend is towards an increasing charging time with distance. Interestingly, for 1.5 m height difference, there is considerable fluctuation at closer distances. The reason for this is the reflection of the EM waves from the ceiling (as the receiver is placed closer to the ceiling), and the peculiar behavior of propagation loss inside a tunnel [19]. This result gives the non-intuitive message that even if a sensor is situated at a greater distance than others, depending upon the location-specific channel behavior, it may still exhibit a better charging rate (e.g. at distances of 4.5 and 7 m for all three heights). Note that for different hardware, these times will differ, and with improvements in RF transfer efficiency, the charging times can be significantly improved which can positively affect the network design. We use our experimental findings as a guideline to develop routing and link layer adaptation at the sensor networks using a similar RF transfer apparatus, as described in the next sections.

## 3.2. Charging-aware route formation

From our experiments, we observed that the charging rate for a given receiver is highly dependent on its specific location and relative height difference with respect to the energy transmitter, ET. Thus, classical metrics such as shortest path, in which all nodes are considered to exhibit a homogenous charging characteristic, do not work well in a realistic setting. Moreover, the residual energy at a sensor may vary during the transmission and re-charging process, and hence this too cannot be a static metric during route formation. The steps of our routing protocol are given as follows.

### 3.3. Route establishment metric

We propose using the charging time (2), measured as the time taken to reach the hardware limited voltage of 1.16 V as the decision metric, as opposed to [17]. First, there is an initialization phase, before the start of the network operation. The ETs transmit continuously for a pre-determined duration, allowing each sensor  $i$  to measure its own charging time,  $t_{ch}^i$ , and the standard deviation  $\eta_{ch}^i$  over multiple trials.

The route formation is initiated by the source node, and our proposed metric can be combined with most existing routing protocols for WSNs. In the current implementation, we modify AODV by including the tuple  $(T_{ch}^{\max}(k), \eta_c^{\max}h(k))$  in the route

request (RREQ) packet that travels over path  $k$ . Here,  $T_{ch}^{\max}(k)$  represents the maximum charging time considering all the nodes currently traversed in the path  $k$ , and  $\eta_c^{\max}h(k)$  is the observed standard deviation for this maximum value. As the RREQ is forwarded by the sensors, they may update the field  $T_{ch}^{\max}(k)$  if their own charging time is greater than the value contained in this field. Thus, for a sensor  $i$ , the change  $T_{ch}^{\max}(k) = t_{ch}^i$  if  $t_{ch}^i > T_{ch}^{\max}(k)$ , is undertaken before broadcasting the RREQ to its neighbors. In addition, the deviation  $\eta_c^{\max}h(k)$  is also included in the packet, whenever the  $T_{ch}^{\max}(k)$  changes, to resolve ties at the destination.

To ensure that the best routes deliver the RREQs first, each node introduces a forwarding delay as a function of its own charging rate. This delay is computed as  $t_{ch}^i + \eta_{ch}^i$ , i.e. the sum of the mean charging time and its deviation of the node divided by a constant factor (e.g. 1000 for delay in the order of ms). It is possible that the best RREQ, the one with the lowest charging time, might not be guaranteed to arrive before the destination node sends out RREP. This is especially true in the case of multiple paths with different numbers of hops. In order to alleviate this issue, the DA scheme has a mechanism that is adaptive to achieve the optimal route, i.e., it keeps track of the best RREQ received and updates the route when necessary, i.e. the destination node sends the new RREP if it receives a RREQ with a lower charging time. This occurs as DA is built atop the classical AODV that incorporates this feature in it by default. This enables the route to sustain its optimality in the DA scheme.

The destination receives multiples RREQs representing the different paths traversed from the source. It now chooses the path, say  $\psi$ , with the lowest value of the maximum charging times of the various paths. Thus,

$$\begin{aligned} \psi &= \min\{T_{ch}^{\max}(k)\} \quad \forall k \\ &= \min\{\max[t_{ch}^i]\} \quad \forall i \in \text{path } k, \forall k. \end{aligned} \quad (1)$$

The destination waits for a time  $T_{setup}$  during the route formation and collects multiple RREQs. Shorter charging times also imply more opportunity for packet transmission, and results in greater throughput. The per-hop delay incurred in the few additional hops in the chosen path is easily offset by the gains in increased network lifetime, as we show in Section 3.1.2.

In practice, the charging time might be affected by many factors, i.e. mobility, and fading. This is particularly true in the mobile WSN with ambient RF energy harvesting. However, the charging time of the system of interest is less exposed to such variations, i.e., energy harvesting mobile WSN powered by dedicated energy transmitters. As with any routing protocols, the DA scheme captures the system state then performs the optimization on the collected data. There is insignificant difference whether the system is dynamic or static since the routing protocol has to make a decision on the instantaneous system state. So it is fair to say that the setup route and duty cycle are optimal with respect to the present state. In order to capture the dynamics of the system, the DA protocol has an adaptive mechanism to deal with the dynamic nature of the system. The adaptive mechanism includes a feature called route invalid masking, which deletes the route if it is non-active. Route invalid masking in the DA algorithm keeps track of active routes and marks ones that are non-active, i.e., each node determines whether its neighbor is considered active for the particular destination. The neighbor of the node is considered active for a particular destination if the neighbor sends a packet or forwards at least one packet for a destination within the active route timeout interval. The charging time deviation during the route setup also has an influence on route expiration since it reflects the dynamic of the system. In the next section, we demonstrate how the charging and transmission durations are optimally decided for the selected path while considering several end-to-end performance metrics.

### 3.4. Charging and transmission time optimization

After the base station chooses the optimal path, it sends back the route reply (RREP) to the nodes of this path, defining the charging ( $T_{ch}$ ) and transmission times ( $T_x$ ) that is common to all of them. Thus, even if a node  $i$  advertised a different value for  $t_{ch}^i$  to charge fully, it must now cease transmission and stay in the charging phase for the entire length specified by  $T_{ch}$ . Our optimization framework given below returns the duration for charging  $T_{ch}$  and the frame length  $T_{frame}$ , where  $T_{frame} = T_{ch} + T_x$ . Once the RREP reaches the source in the return path, all the nodes are initialized and the network can now begin forwarding the data packets:

Given :  $L_{lim}, ESR_{lim}, N$

To find :  $T_{ch}, T_{frame}$  (2)

To Maximize : Throughput =  $\frac{T_x \cdot R}{T_{frame}}$

Subject to :

$$(E_{rec} - E_{idle}) \cdot T_{ch} - E_{tx} \cdot T_x \geq 0 \quad (3)$$

$$N \left( T_{ch} + \frac{P + H}{R} \right) \leq L_{lim} \quad (4)$$

$$\frac{1}{ESR_0} \left[ 1 - k \cdot t \cdot \exp^{-\frac{4700}{T+273}} \right] > \frac{1}{ESR_{lim}} \quad (5)$$

$$T_{frame} = T_x + T_{ch}. \quad (6)$$

The aim of this optimization framework is to maximize the throughput subject to several constraints. As the node can only transmit during the transmission times, and must remain silent during the charging times, the throughput is expressed as the ratio of total number of bits sent during  $T_x$  to the frame time  $T_{frame}$ . The end-to-end latency limit  $L_{lim}$  and the capacitor quality metric  $ESR_{lim}$  are specified based on application and device lifetime requirements. Finally,  $N$  is the total number of nodes in the path. In order to find the charging time  $T_{ch}$  and the frame time  $T_{frame}$  that maximizes the throughput, we define the constraints as follows:

- The constraint of keeping the sensor alive after each frame duration is reflected in (3). Here, the sensor expends idle energy  $E_{idle}$  during its charging time. This is a function of the internal circuit operation of the sensor. However, it gains energy at the rate  $E_{rec}$  from the wireless transmitter in this duration  $T_{ch}$ . In addition, during the transmission duration the sensor loses energy at the rate  $E_{tx}$  due to sending and receiving packets. Thus, after the frame duration, the residual energy must at least be greater than 0.
- The end-to-end latency of a packet for the  $N$  hop route must be below a pre-decided limit  $L_{lim}$  as given in (4). This can be a function of the type of application and the nature of the data expected from the network. At each hop, in the worst case, a sensor may experience a delay equal to the charging time  $T_{ch}$  in which no data can be sent and the transmission delay which is given by the ratio of the packet size  $P$  combined with the header size  $H$  and the sending rate  $R$ .
- Equivalent series resistance (ESR) is a metric that is used to determine the operational quality of the capacitor. Over time, the ESR increases, and once it is beyond the limit  $ESR_{lim}$ , the capacitor is considered dysfunctional. The capacitor lifetime constraint is captured in (5), where  $T$  is the absolute temperature in Kelvin at which the capacitor operates,  $t$  is the operational time, and  $k$  is a design constant. The capacitor is subjected to a charging voltage only during the interval  $T_{ch}$  in each frame. Thus, if  $\mu$  is the target network lifetime in terms of the number of completed frames, then the effective operational time of the capacitor is  $t = \mu \cdot T_{ch}$ .
- Finally, the constraint (6) gives the relationship between the charging and transmission times and the frame time.

#### 4. Device-specific protocol

In the device-specific (DS) approach, we model the integrated energy harvesting module and sensor mote (as shown in Fig. 1(a)) through precisely constructed equations as part of the *device characterization*. These equations exactly state the capacitor voltage (hence, residual energy) during the energy harvesting and sensor transmission durations, which are obtained from the determination of the *link layer duty cycles*. Finally, the *routing protocol* helps in choosing the best route among the candidate paths.

##### 4.1. Device characterization

We undertake this study in two steps, i.e., develop analytical models for the *charging* and *operational* phases of the sensor.

###### 4.1.1. Charging phase

We obtain the relationship between the received power  $\mathcal{P}$ , the capacitor  $\mathcal{C}$  that will be charged by the energy harvesting device, and the output voltage  $V$  up to which the capacitor can be charged through real measurements of our energy harvesting equipped sensor. The classical approach of using the power and voltage relationship of the capacitor, i.e.,  $\mathcal{V} = \mathcal{V}_0(1 - e^{-\frac{t}{RC}})$  cannot be directly applied to obtain the charging time  $t$ . This is because the harvesting circuit is composed of non-linear and reactive components (Schottky diodes, inductors and capacitors) whose efficiency and reactance vary with the incident signal or power level. Several additional circuit enhancements exist, such as dynamically switching between multiple stages of the basic voltage multiplier circuit which cannot be obtained from a simple study of the circuit. Moreover, our multivariable function allows the network designer the flexibility in choosing the energy storage capacitor based on application environments.

We used the Powercast P2100 as the energy harvesting device and a Agilent Technologies N5181A signal generator to feed in varying signal power levels from  $-20$  to  $17$  dBm. We also varied the storage capacitor size from  $1 \mu F$  to  $220$  mF, and measured the time taken to charge to the maximum voltage output from the harvesting module ( $3.3$  V). For each capacitor size, the voltage–time curve was logged for varying input power levels. We begin with the equation  $V = a_1 e^{a_2 t} + a_3 e^{a_4 t}$ , which gives the voltage at the capacitor when the harvesting circuit is in use for time  $t$ , all other node operations being suspended. We base this choice by implementing a family of different functional approximations in MATLAB, and testing for the least square error (MSE) criterion. Interestingly,  $a_1$  and  $a_3$  turned out to be constant with the variation of  $P$ , but the terms  $a_2$  and  $a_4$  were exponential functions themselves for the best fit using the LSE criterion. Coefficients  $a_1$ ,  $a_3$ ,  $a_4$  and  $a_6$  did not show any changes with respect to  $\mathcal{C}$  in the curve fitting process, and were kept constant. However, coefficients  $a_2$  and  $a_5$  were inversely proportional to  $\mathcal{C}$ . Hence, the final form of the equation is given in (7):

$$\mathcal{V} = f(\mathcal{P}, \mathcal{C}, t) = a_1 e^{a_2 \frac{t}{\mathcal{C}} e^{a_3 \mathcal{P}}} + a_4 e^{a_5 \frac{t}{\mathcal{C}} e^{a_6 \mathcal{P}}} . \quad (7)$$

From (7) and using the Gauss–Newton optimization method [20], an approximation of coefficients  $a_i$  were calculated as  $\{32.62, 2.38e - 5, 0.23, -30.86, 2.35e - 5, 0.23\}$ , respectively, for  $i = 1, \dots, 6$ . The functional representation of the charging phase is shown in Fig. 3(a).

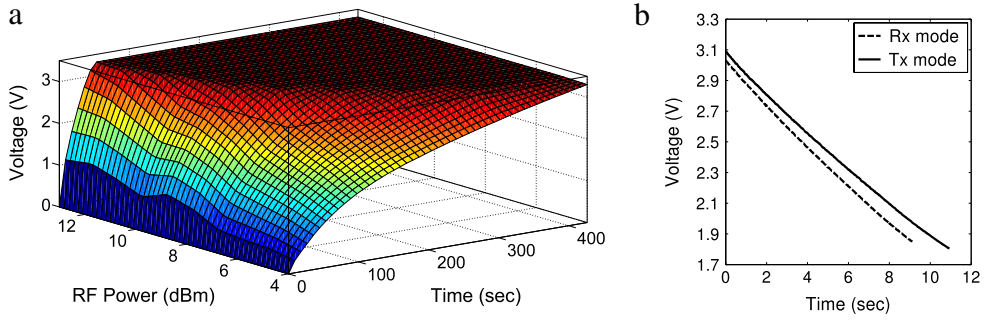


Fig. 3. The functional representation of the charging phase (a) and the energy loss during transmission and reception (b).

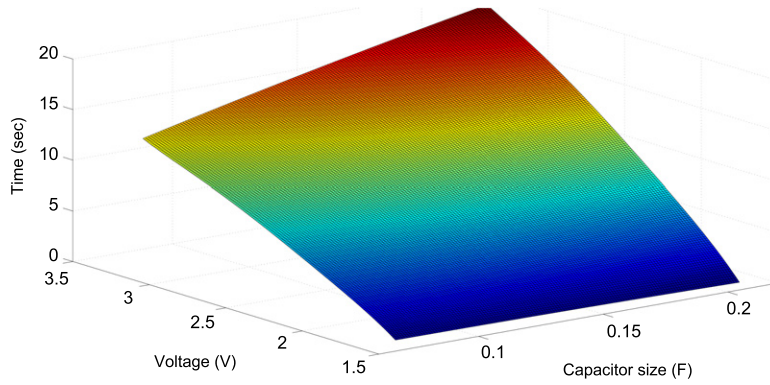


Fig. 4. The effect of capacitor sizes during capacitor discharging.

#### 4.1.2. Operational phase

Power consumption of the sensor is different during transmission and reception. Additionally, since the storage capacitor that powers the node during its operation is not a fixed voltage source, the voltage across it drops until it reaches a point, here 1.8V, where the sensor stops operating. Fig. 3(b) shows the voltage level drop on a 100 mF capacitor versus time, consumed by a Mica2 mote for transmission-only (at  $-20$  dBm) and reception-only modes.

To characterize the energy loss during transmission, two Mica2 sensor motes running TinyOS 2.1.0 were used as a sender–receiver pair. The transmitting mote used only the stored energy in the capacitor. The packets contained the source node ID, time-stamp, sequence number, and voltage level of the sender's capacitor, and were continuously sent till the node shut down because of energy depletion. Fig. 4 illustrates the discharging characteristic of the sender node under 3 different capacitor sizes (82, 100, 220 mF). At the receiver side, a similar study was undertaken, where the mote was powered only from the charged capacitor and programmed to receive packets until the shut down voltage 1.85 V was reached. Then, all the received packets are written to the non-volatile EEPROM memory before shutting down. At the next bootup, the sensor transfers these packets to the host computer via a base station. Using these measurements, we estimate the residual time to energy depletion of a node due to reception ( $\mathcal{T}_{rx}$ ) and transmission ( $\mathcal{T}_{tx}$ ) alone, respectively, as follows:

$$\mathcal{T}_{rx}(\mathcal{C}, \mathcal{V}) = -13 - 87.5\mathcal{C} + 9.3\mathcal{V} + 47.7\mathcal{C}\mathcal{V} - 1.3\mathcal{V}^2 \quad (8)$$

$$\mathcal{T}_{tx}(\mathcal{C}, \mathcal{V}) = -17.3 - 60.8\mathcal{C} + 12.2\mathcal{V} + 34.7\mathcal{C}\mathcal{V} - 1.5\mathcal{V}^2. \quad (9)$$

#### 4.2. Link layer duty cycles

In this section, we calculate the charging time  $T_{ch}$  and the transmission time  $T_x$  that are used by all the nodes of the network.

First, each sensor undertakes a one-time reporting of the level of received power (say, from the external energy transmitter) to the base station. If direct feedback is infeasible, which is possible for very large networks, then the average received power at each node can be calculated by knowing the transmitter locations and using an appropriate path loss model. Fig. 5 shows the analytically calculated probability density function (PDF)  $\mathbb{P}$  of the received harvesting power in a network of 30,000 nodes in a  $300 \times 300$  area where a  $10 \times 10$  grid of 3 W energy transmitters is present.

Next, we formulate a framework that finds the best values for the storage capacitor value  $\mathcal{C}$  and the voltage  $\mathcal{V}$  up to which the capacitor must be recharged, so that the useful transmission time is optimized. Thus, we can formally express

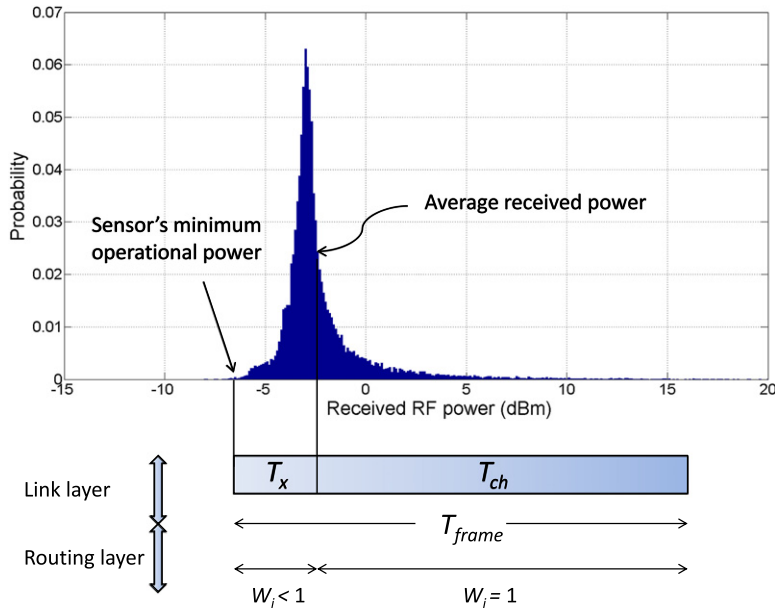


Fig. 5. The PDF of the received energy levels of the entire WSN, and the choice of the charging–transmission cycle.

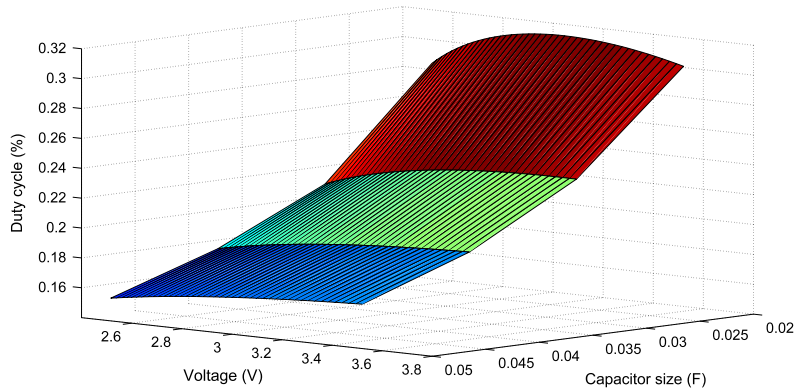


Fig. 6. The effect of non-optimal capacitor size and voltage on the duty cycle of the DS protocol.

this calculation as:

$$\{c, v\} = \arg \max_{c, v} \int_{\mathcal{P}_{\min}}^{\mathcal{P}_{\max}} \mathbb{P} \frac{T_{rx}(c, v) + T_{tx}(c, v)}{f'(\mathcal{P}, c, v)} d\mathcal{P}. \tag{10}$$

The above equation is derived from (7) and (9), which respectively denote the charging time, and useful transmission time. The transmission time itself can be equally used between packet sending and receiving at a given node, and hence, we take the average residual time accounting for both of these factors. Moreover, as the received power itself is not a constant for all nodes, we consider a range of values given by the PDF  $\mathbb{P}$  under the boundary conditions of minimum ( $\mathcal{P}_{\min}$ ) and maximum ( $\mathcal{P}_{\max}$ ) received powers, respectively. Finally,  $T_{ch} = f'$  is the inverse of  $f$ , and it gives the time taken to charge the capacitor to the upper limit of 3.3 V. This inverse is computed numerically from (7) using MATLAB.

Solving the above equation for the same sample scenario used to generate the PDF in Fig. 5, we get  $\{c, v\} = \{0.02 \text{ F}, 3.0 \text{ V}\}$ . These values, in turn, result in  $T_{ch} = 628.2$  and  $T_x = 1.97$  s, respectively.

The results from the optimization are the optimal capacitor size and the charging voltage. This implies that the sensor will operate with the optimal duty cycle if these parameters are in effect. However, it is important to observe the effect of deviation in capacitor size and charging voltage on the duty cycle. Consequently, the capacitor size and charging voltage are varied to observed the duty cycle. Fig. 6 shows the duty cycle under various capacitor size and charging voltage. It is obvious that the duty cycle is maximized at the capacitor size of 20 mF and the charging voltage of 3.0 V, which was derived from the optimization mentioned earlier. Note that 20 mF is the lowest capacitor size that renders Mica2 operational in practice. It is also clear that changes in parameters do not significantly affect the duty cycle rather than yielding a sub-optimal duty cycle.

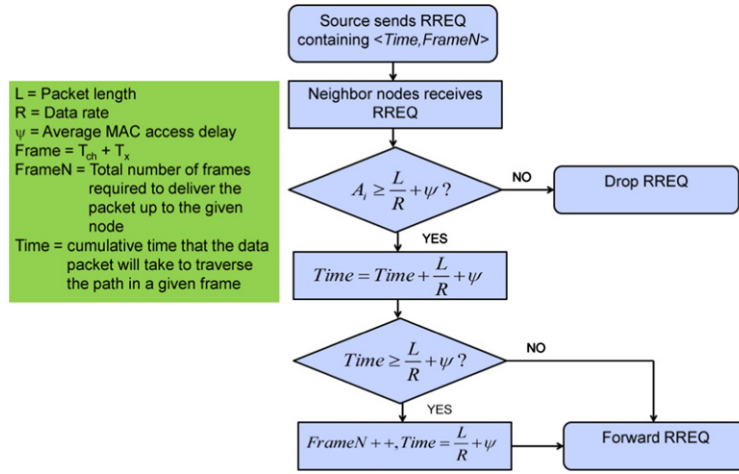


Fig. 7. The flow diagram of the RREQ-forward procedure.

### 4.3. Routing protocol

In the previous section,  $T_x$  was chosen for the entire network. However, nodes with receive power levels significantly lower than the average given by the distribution of  $\mathbb{P}$  are likely to run out of energy before this duration  $T_x$  is completed.

In order to decide a node's suitability to participate in the route, we measure the time actually left for the node's operational phase (based on the residual energy and node-specific conditions). Formally, this actual time for transmission, called the *active time*  $\mathcal{A}_i$  for the node  $i$ , is

$$\mathcal{A}_i = \min \left\{ T_x, \frac{\mathcal{T}_{rx}(\mathcal{C}, \mathcal{V}) + \mathcal{T}_{tx}(\mathcal{C}, \mathcal{V})}{2} \right\}. \quad (11)$$

We assume here that a node spends equal time receiving and sensing packets. A node with higher active time is preferred to forward the packet among potential relay nodes. Note that  $\mathcal{T}_{rx}(\mathcal{C}, \mathcal{V})$  and  $\mathcal{T}_{tx}(\mathcal{C}, \mathcal{V})$  are calculated based on the values derived in Section 4 for  $\mathcal{C}$  and  $\mathcal{V}$ , respectively.

The source sends out a modified route request (RREQ) packet during route formation. Each sensor may forward the RREQ only if the active time is sufficient to transmit a data packet of length  $L$  under a pre-determined rate  $R$ . Hence, the packet is forwarded if  $\mathcal{A}_i \geq \frac{L}{R} + \psi$ , where  $\psi$  is the average observed MAC layer channel access delay, and  $\frac{L}{R}$  is the packet transmission time. This step is shown in the first conditional test block in Fig. 7. Further, the RREQ has two additional fields given by the tuple  $\langle \text{Time}, \text{FrameN} \rangle$ .  $\text{Time}$  contains the cumulative time that the data packet will take to traverse the path in a given frame, where a frame is defined as the duration  $T_{ch} + T_x$ . The  $\text{FrameN}$  field gives the total number of frames required to deliver the packet up to the given node. This is a key metric as the charging times  $T_{ch}$  are indeed lengthy (hundreds of seconds), and these durations that render the sensor incapable of data forwarding are present in every frame. If the first conditional test block is true, the node calculates the total delay in the current frame, i.e., the sum of the previous value of  $\text{Time}$  and the current link delay  $D$ , defined as  $\frac{L}{R} + \psi$ . If this time is greater than the maximum possible active time, then the  $\text{FrameN}$  count is incremented by one, indicating that the packet now needs to wait for the next transmission duration. In this case,  $\text{Time}$  is reset to reflect the time elapsed in the current frame only.

The destination chooses the route that takes the minimum number of elapsed frames to deliver the packets, i.e., the minimum value of  $\text{FrameN}$ . As the time of arrival of the RREQ does not reflect the final path chosen, each forwarding node, as well as the destination, must continue to accept RREQ packets even if an earlier one has already been processed for a pre-determined duration  $\delta$ .

## 5. Performance evaluation

In this section, we thoroughly evaluate our proposed approach using the ns-2 simulator. A total of 200 nodes were randomly deployed in a  $100 \text{ m} \times 100 \text{ m}$  area. The sensors operate in the lowest power consumption state, using  $-20 \text{ dBm}$  for transmission power to maximize their lifetimes. This, however, results in the tradeoff of  $10 \text{ m}$  operational range using the free space path loss model. Fig. 8(a) shows the topology used in the study with the 3 W energy transmitters (ETs) arranged in a grid. The WSNs form chains with the source at one end and the sink located at the top right corner, and the total area of deployment is a square of side  $100 \text{ m}$ . The preliminary study on the DA scheme appeared in the shorter version of this paper [13]. However, we present completely new results and metrics that serve to compare the two approaches. Importantly, the energy model used is thoroughly revised based on actual measurements described in Sections 4.1 and 4.1.2, respectively. For the purpose of comparison, we have also implemented a *voltage-aware* AODV-based scheme (VA) [17] which was described in Section 2.

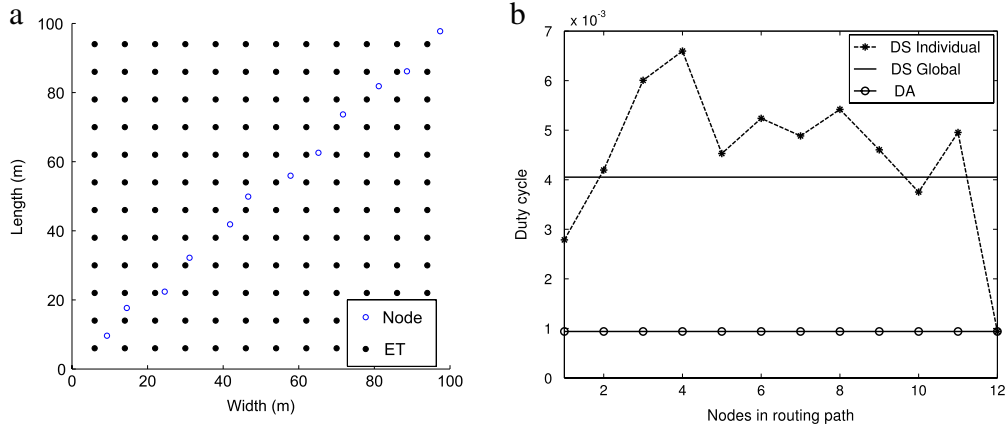


Fig. 8. A 12 × 12 energy transmitter grid and a chain of sensor nodes (a). A comparison of the duty cycles between the DA and DS schemes (b).

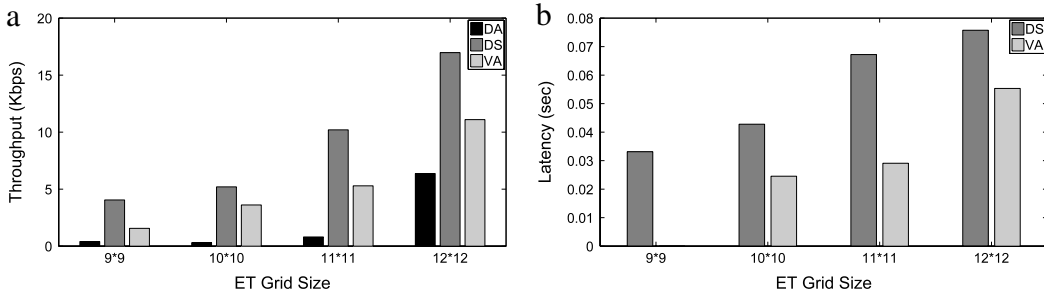


Fig. 9. Throughput (a) and delay (b) comparison of routing schemes with varying ET grid size.

5.1. Comparison of duty cycles

Consider a single diagonal route shown in Fig. 8(a). Fig. 8(b) shows the calculated duty cycle on this route using Device-Agnostic (DA) and Device-Specific (DS) schemes. The broken line shows the individual duty cycles calculated for the sensors along the 12-node path in the DS scheme. However, the DS scheme decides one network-wide fixed duty cycle, using the calculations in Section 4.2, which is shown by the solid line. This is the average value of the duty cycle for all the nodes within the network. Intuitively, the duty cycle in the DS scheme is much higher than that for the DA scheme, as the latter is decided by the duty cycle of the node having the longest charging time in the path (Section 3.4).

5.2. Effect of the number of energy transmitters

We vary the number of ETs deployed in the network in the range 9 × 9 to 12 × 12 arranged as a regular grid while keeping the area size constant. This increase in the number of ETs allows nodes to harvest more energy. Fig. 9(a) and (b) show the effect of varying the ET grid size on the throughput and packet latency in 3 different schemes, including Device-Agnostic (DA), Device-Specific (DS) and Voltage-Aware (VA). The DS scheme delivers the highest throughput among these three, while the DA scheme yields the lowest throughput. The delay of the DA scheme was considerably larger, in the order of tens of seconds (owing to very low duty cycles, as seen in Fig. 8(b)) and was removed from Fig. 9(b) for the sake of visibility and comparison between the DS and VA schemes.

5.3. Effect of the network load

The rate of data packets loaded to the network, called network load, was varied from 2.4 to 38.4 Kbps in this study. In Fig. 10(a), we observe a distinct increasing trend for both DS and VA schemes, although DS performs better than VA. However we observe that the DA scheme not only yields significantly less throughput but also shows no major change in throughput with increasing load. This is because in the given optimization, the optimized charging time is calculated based on a signal rate and also to gain sufficient charge to send only one packet at a time. Fig. 10(b) shows the latency comparison of the DS scheme against the VA. The DA latency is again not shown for the purpose of visibility, as it is much higher than both DS and VA. It is shown that the VA yields a marginally lower latency than DS. However, the difference in latency decreases as the load produced increases. Moreover, at the highest load produced, both schemes yield insignificant difference in terms

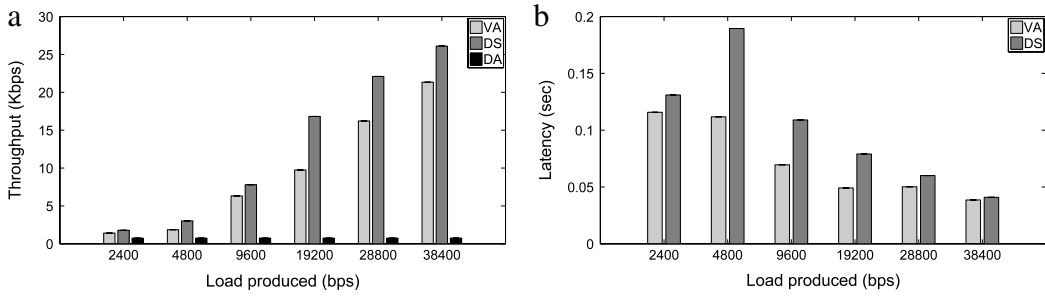


Fig. 10. Throughput (a) and delay (b) comparison of routing schemes with varying load from source node injected to the network.

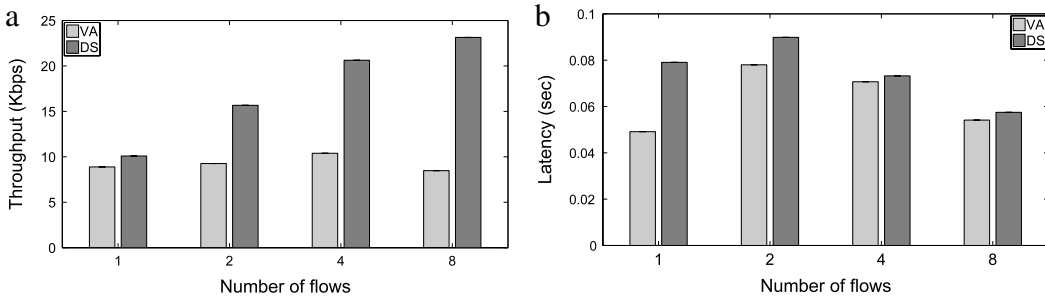


Fig. 11. Throughput (a) and delay (b) comparison of routing schemes with varying number of data flows.

of latency. We believe that at the highest load produced, the network is saturated and the behavioral aspect of both DS and VA is overwhelmed by the limited data rate of Mica2's radio, 38.4 Kbps. In most applications where throughput is of most concern, the gain increase in throughput of the DS scheme over the VA scheme can easily offset the marginal latency introduced by DS.

#### 5.4. Effect of multiple flows

The effect of multiple simultaneous flows in the network was investigated, between randomly selected source nodes and destinations. We vary this number of flows from 1, 2, 4 and 8. Fig. 11(a) and (b) show the effect of such variation on the throughput and average packet delay in the network. Recall that the DA scheme relies on the entire path having one duty cycle, and multiple flows that cross each other adversely affect the performance of the DA scheme. Hence, this study is focused on evaluating the performance of the DS and VA schemes. Fig. 11(a) shows that throughput increases for the DS scheme while the VA scheme does not show a major change with increasing number of flows. We interpret this behavior as follows: in the DS scheme, a path composed of nodes with high recharging ability are picked, therefore those nodes can serve more numbers of flows during their active transmission times. But since in the VA method only the instantaneous voltage of nodes is used as a routing metric, this does not represent their available voltage at later times when the nodes harvest the ambient energy. Hence, during the actual network operation, there is no observed correlation in the throughput with increasing number of flows for the VA scheme. The latency of DS and VA schemes is shown in 11(b). The DS scheme yields a minimally higher latency than the VA scheme. The difference in latency among both schemes is less pronounced as the number of flows increases. We explain the phenomenon as follows. As the number of flows increases, more nodes in one flow also belong to other flows. This results in premature energy depletion of the nodes that participate in multiple flows.

In summary, we observe that in all the cases where throughput was studied, the DS method performs the best. This is because it chooses the path with the lowest number of frames  $Frame_N$ , i.e., a path that delivers the packets to the destination as fast as possible.

## 6. Conclusion

We proposed two cross-layered protocols for Energy Harvesting Networks, Device-Agnostic (DA) and Device-Specific (DS). A thorough performance evaluation was conducted with various important metrics, including duty cycles, number of energy transmitters, network load and multiple flows. The duty cycle of the DS scheme is much higher than that of the DA scheme. In most applications where throughput is of most concern, the DS scheme is preferable over DA and VA schemes due to the higher throughput yielded. The DS scheme also yields marginally higher latency than the VA scheme. However, the significantly higher throughput of the DA scheme can easily offset the marginal latency incurred. On the other hand, the

lower latency of the VA scheme makes it suitable for applications where the lowest latency is required. The lowest latency requirement becomes insignificant as the network converges to the saturation point, i.e. the data rate of the radio employed.

## Acknowledgment

This material is based upon work supported by the US National Science Foundation under Grant No. CNS-1143681.

## References

- [1] I.F. Akyildiz, W. Su, Y. Sankarasubramaniam, E. Cayirci, *Wireless sensor networks: a survey*, *Computer Networks (Elsevier)* 38 (4) (2002) 393–422.
- [2] S.N. Pakzad, G.L. Fennes, S. Kim, D.E. Culler, Design and implementation of scalable wireless sensor network for structural monitoring, *ASCE Journal of Infrastructure Engineering* 14 (1) (2008).
- [3] US Energy Information Administration, *International Energy Outlook—DOE/EIA-0484*, 2010, [Online]. [www.eia.gov/oiaf/ieo/index.html](http://www.eia.gov/oiaf/ieo/index.html).
- [4] V. Raghunathan, S. Ganeriwal, M. Srivastava, Emerging techniques for long lived wireless sensor networks, *IEEE Communications Magazine* 44 (4) (2007) 108–114.
- [5] P.H. Chou, S. Kim, Techniques for maximizing efficiency of solar energy harvesting systems (invited paper), in: *Proceedings of the Conference on Mobile Computing and Ubiquitous Networking*, ICMU, Seattle, WA, Apr 2010.
- [6] T. Senjyu, Y. Ochi, Y. Kikunaga, M. Tokudome, A. Yona, E.B. Muhando, N. Urasaki, T. Funabashi, Sensor-less maximum power point tracking control for wind generation system with squirrel cage induction generator, *Renewable Energy (Elsevier)* 34 (4) (2009) 994–999.
- [7] S.X. Dong, J. Zhai, J.F. Li, D. Viehland, S. Priya, Multimodal system for harvesting magnetic and mechanical energy, *Applied Physics Letters* 93 (10) (2008).
- [8] P. Li, Y. Wen, P. Liu, X. Li, C. Jia, An electromagnetic energy harvesting circuits for self-powered wireless sensor network, *International Conference on Control, Automation, Robotics and Vision*, Hanoi, Vietnam, Dec 2008.
- [9] T. Paing, J. Shin, R. Zane, Z. Popovic, Resistor emulation approach to low-power RF energy harvesting, *IEEE Transactions on Power Electronics* 23 (3) (2008) 1494–1501.
- [10] P. Nintanavongsa, U. Muncuk, D.R. Lewis, K.R. Chowdhury, Design optimization and implementation for RF energy harvesting circuits, *IEEE Journal on Emerging and Selected Topics in Circuits and Systems* 2 (1) (2012) 24–33.
- [11] Powercast Corporation, P2000 Series 902–928 MHz Powerharvester Development Kit, [Online]. <http://www.powercastco.com/products/development-kits/>.
- [12] Z.A. Eu, W.K. Seah, H. Tan, A study of MAC schemes for wireless sensor networks powered by ambient energy harvesting, *IEEE International Conference on Industrial Informatics*, pp. 1030–1035, Aug 2006.
- [13] R. Doost, K. Chowdhury, M. Di Felice, Routing and link layer protocol design for sensor networks with wireless energy transfer, *IEEE Globecom*, 2010.
- [14] A. Bogliolo, S. Delperiori, E. Lattanzi, A. Seraphiti, Self-adapting maximum flow routing for autonomous wireless sensor networks, *Springer Cluster Computing Journal* (2010).
- [15] D. Noh, I. Yoon, H. Shin, Low-latency geographic routing for asynchronous energy-harvesting WSNs, *Journal of Networks* 3 (1) (2008) 78–85.
- [16] S. Mahlknecht, S.A. Madani, M. Roetzer, Energy aware distance vector routing scheme for data centric low power wireless sensor network, *IEEE International Conference on Industrial Informatics*, pp. 1030–1035, Aug 2006.
- [17] K. Pappa, A. Athanasopoulos, E. Topalis, S. Koubias, Implementation of power aware features in AODV for ad hoc sensor networks, a simulation study, in: *Proceedings of IEEE Emerging Technology and Factory Automation*, Apr 2007.
- [18] A. Kansal, J. Hsu, S. Zahedi, M. Srivastava, Power management in energy harvesting sensor networks, *ACM Transactions on Embedded Computing Systems* 6 (4) (2007).
- [19] I.F. Akyildiz, Z. Sun, M.C. Vuran, Signal propagation techniques for wireless underground communication networks, *Physical Communication (Elsevier)* 2 (3) (2009) 167–183.
- [20] R. Fletcher, *Practical Methods of Optimization*, second ed., Wiley, ISBN: 978-0-471-49463-8, 2000.